Dynamics Analysis of Water Ditching of Deformable Helicopter

Sun Xuan[1], *Tong Mingbo*[1*], *Wang Zhengzhong*[2]

1. Ministerial Key Discipline Laboratory of Advanced Design Technology of Aircraft, Nanjing University of Aeronautics and Astronautics, Nanjing 210016, P. R. China;
2. Science and Technology on Rotorcraft Aeromechanics Laboratory, China Helicopter Research and Development Institute, Jingdezhen 333001, P. R. China

(Received 21 November 2015; revised 22 March 2016; accepted 28 April 2016)

Abstract: To understand the effect of attitude angle on helicopter water ditching, a finite element model (FEM) of helicopter water ditching was established via the nonlinear finite element method. Based on the LS-DYNA software, the finite element model of the helicopter was established. Different attitude of helicopter water ditching was simulated and analysed. Three pressure measuring points were arranged in the aircraft belly area. The pressure curves were provided seperately. Finally, the effects of attitude on helicopter water ditching was discussed, particularly the stability and the overload of helicopter. Through the contours of stress, it can be figured out that the maximum pressure locates at the position of aircraft belly where stiffness is larger. Then simulation and experimental results were compared. The difference of peak acceleration along the Z direction was small. Therefore, this method is feasible and helpful for the design of helicopter water ditching.

Key words: water ditching; helicopter; LS-DYNA; SPH method

CLC number: V215.2 **Document code**: A **Article ID**: 1005-1120(2017)06-0720-13

0 Introduction

Helicopter water ditching is different from fixed-wing aircraft. The fixed-wing aircraft has a large cargo compartment in the bottom, which can absorb impact energy. The wing can also provide floating volume for low-wing plane. Meanwhile, the center of gravity is in the lower part of fuselage, which is conducive to the stability of aircraft on the water. However, the center of gravity of helicopter is generally higher. Ditching may cause the helicopter rollover, leading to accidents. Because of limited volume under floor, the ability of helicopter to absorb impact energy is poor.

The landing gear of the helicopter can absorb energy in ground crash, but in water ditching, the landing gear is useless.

When ditching, the load distribution on the helicopter structure is completely different from that on ground crash, as shown in Fig. 1.

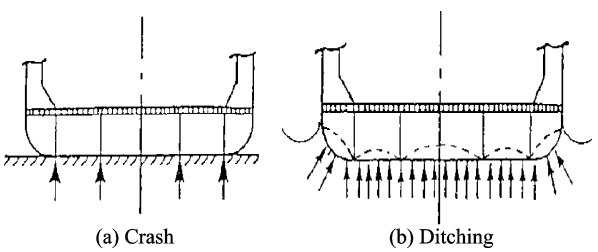

Fig. 1 Load distribution on structure of crash and ditching

In the case of ground crash, the helicopter's beam and frame structure of belly can absorb a large number of impact energy. While ditching on water, the main load is equipped on the belly skin, which is easy to fracture because of such large impact energy.

Traditional research method for helicopter water ditching is experiment, which can verify whether or not the requirements are met. For example, the full scale WG30 water ditching experi-

* Corresponding author, E-mail address: aspb@nuaa.edu.cn

How to cite this article: Sun Xuan, Tong Mingbo, Wang Zhengzhong. Dynamics analysis of water ditching of deformable helicopter[J]. Trans. Nanjing Univ. Aero. Astro., 2017,34(6):720-732.
http://dx.doi.org/10.16356/j.1005-1120.2017.06.720

ment[1] was carried out. The experiment was designed by WESTLAND Corporation. The helicopter is 14.23 m long, 3.04 m wide and 3.1 m high. The materials are mainly aluminum alloy and titanium alloy. WG30 contains 10 passenger seats, a pilot seat, a rotor rotating system, and two engines. The mass of structure is 3 000 kg. There are 21 acceleration sensors and 12 pressure sensors placed on the helicopter.

With the development of computer technology, CAE technology has become more mature. A large number of simulations have been carried out abroad for various scientific issues. Since 1990s, an important development of water ditching simulation is the application of finite element technology. The maturity of the finite element technique makes it possible to analyze the structure and fluid coupling. The complex 3D geometry, the nonlinear free surface, the compressibility of water and the deformation of the structure can be considered at the same time. Using the software LS-DYNA, Brooks and Anderson[2] simulated the water ditching of Apollo re-entry module. Streckwall[3] studied the free surface and the free movement of water when aircraft is ditching using the smoothed particle hydrodynamics (SPH) method. In 2009, Nathalie[4] also applied this method to the ditching of helicopter. Results showed that it was feasible. Paul[5] used the PAM-CRASH to establish water wave.

In recent years, domestic researchers have looked into the research of fluid-solid coupling with SPH method and any Lagrange-euler(ALE) method. Guo[6] focused on the mechanical performance of the hybrid wing-body configuration aircraft SAX-40. They concluded that the aircraft had unstable trend of jumping off water. Using ALE method, Fang[7] simulated water ditching of fixed-wing aircraft, and got some overload curves. Based on SPH method, Yan[8] simulated water ditching of fixed-wing aircraft and got the results that 12 degrees of pitch angle and landing gear raised was the best state of ditching. Based on ALE method, Zhu[9] obtained the maximum stress anddamage area of fuselage. Shen[10] designed airbag buffer system of lunar probe then simulated the buffer process, which could reduce the overload of the lunar probe effectively. Using LS-DYNA, based on ALE method, Li[11] simulated water ditching of helicopter, resulting in some useful conclusions. Sun[12] established a certain type of aircraft rigid body and elastic body, using SPH method to show the water splashing.

Based on LS-DYNA, the finite element model of the helicopter was established in this paper. Different attitude of helicopter water ditching was simulated. Three pressure measuring points were arranged on the aircraft belly. The effects of attitude on helicopter water ditching was analyzed.

1 Theory of SPH

1.1 Explicit solution

Since water ditching includes geometric nonlinearity, material nonlinearity and contact-boundary nonlinearity, simulation can only use a very small time step. A simulation algorithm is required to convert the nonlinear stiffness matrix when using implicit solution, which causes it difficult to guarantee the convergence of large nonlinear problem. However, explicit simulation algorithm can directly solve the problem by noncoupled equations. It does not require the transformation of stiffness matrix, which is more suitable for ditching problem. Therefore, the central difference method[13] is used.

The step is divided by n and time step Δt^n in the time domain. $d^n = d^n(t^n)$ is the node displacement. Time increment is defined as follows

$$\Delta t^{n+\frac{1}{2}} = t^{n+1} - t^n, t^{n+\frac{1}{2}} = \frac{1}{2}(t^{n+1} + t^n)$$

$$\Delta t^n = t^{n+\frac{1}{2}} - t^{n-\frac{1}{2}} \tag{1}$$

Velocity difference formula is defined as follows

$$V^{n+\frac{1}{2}} = \frac{d^{n+1} - d^n}{t^{n+1} - t^n} = \frac{1}{\Delta t^{n+\frac{1}{2}}}(d^{n+1} - d^n) \tag{2}$$

Integral form is defined as follows

$$d^{n+1} = d^n + \Delta t^{n+\frac{1}{2}} v^{n+\frac{1}{2}} \tag{3}$$

Acceleration is defined as follows

$$a^n = \frac{\Delta t^{n-\frac{1}{2}}(d^{n+1} - d^n) - \Delta t^{n+\frac{1}{2}}(d^n - d^{n-1})}{\Delta t^{n+\frac{1}{2}} \Delta t^n \Delta t^{n-\frac{1}{2}}} \tag{4}$$

The time integration equations of the impact motion can be expressed as

$$Ma^n = f^n = f^{\text{ext}}(d^n, t^n) - f^{\text{int}}(d^n, t^n) \quad (5)$$

where M is the mass, f^{ext} the external node force, f^{int} the internal node force. Boundary condition is expressed as

$$g_i(d^n) = 0 \quad (6)$$

$$v^{n+\frac{1}{2}} = v^{n-\frac{1}{2}} + \Delta t M^{-1} f^n \quad (7)$$

Under the boundary conditions, the displacement of node d^n is known. The nodal force f^n is determined by the constitutive equation and the nodal force equation. Therefore, the node displacement can be determined by the formula. Thus, the displacement, strain and stress can be solved.

But it should be noted that the explicit central difference method is conditionally stable algorithm. Every time step should not exceed the critical time step size.

1.2 SPH method

SPH method[14] is a mesh free method. The idea of this method is to describe the continuous fluid with the particle group. Each point contains a variety of physical quantities, including mass, speed, etc. The mechanical behavior of the whole system is obtained by solving the dynamic equation of the particle group. The mechanical process can be accurately described as long as the number of particles is enough. There is no grid relationship between particles, so it can avoid the distortion of the mesh with large deformation.

The domain is represented by a series of random particles. The initial particles are evenly arranged usually. The field function is approximated by the integral representation method, which is called kernel approximation in the SPH method.

The integral expression of the neighboring particles in the support domain is used to calculate the expression of the field function, so the SPH method is adaptive.

The particle approximation is applied to the field function of all partial differential equations. Then discretize the differential equation of particles. It is a pure Lagrange method. Finally, the variation values of the field variables of all particles are obtained by using the explicit integration method.

The SPH method is based on kernel estimation, which is based on function

$$A(r) = \int A(r')\ \delta(r - r')\mathrm{d}r' \quad (8)$$

The integral approximate expression is

$$\langle A(r) \rangle = \int A(r')\ w(r - r', h)\mathrm{d}r' \quad (9)$$

where W is the kernel function, which is used to generate an estimate to filter the local fluctuations. Kernel W should satisfy function as follows

$$w(r, h) = \left(\frac{1}{h\sqrt{\pi}}\right)^d \mathrm{e}^{-\frac{r^2}{h^2}} \quad (10)$$

$$\int_D w(r - r', h)\mathrm{d}r' = 1 \quad (11)$$

Since the SPH method is not restricted by grid continuity, it is possible to simulate splash accurately than the ALE method.

2 Mesh Refinement

A hemisphere drop vertical onto cylindrical shape of water, which use penalty function method as contact algorithm[15]. The simulation and experimental data[16] are compared. Then the sensitivity of grid was studied. Simulation is carried out using international closed unit.

2.1 Parameters of model

The parameters of hemisphere and the water region are shown in Table 1. The grid size of the hemisphere is 0.005 m. The number of nodes is 4 602, and the number of cells is 4 618.

Table 1 Parameters of hemisphere and water

Parameter	Value
Diameter of water/m	0.660 4
Depth of water/m	0.381
Diameter of hemispheric/m	0.203 2
Mass of hemispheric/kg	29
Vertical velocity/(m · s^{-1})	7.62
Time/s	0.03

The different particle size was studied in order to identify the influence of the particle size,

which are shown in Table 2 and Fig. 2.

Table 2 Particle size and element number

Diameter of particle/m	Element number
0.015	38 200
0.010	130 568
0.005	1 040 592

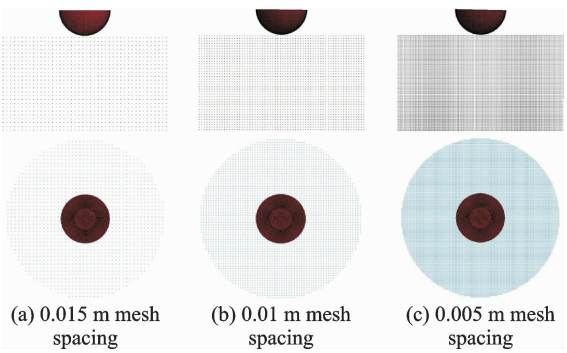

Fig. 2 Different particle size

2.2 Results

The experimental result in the literature, and the simulation results of 0.015 m, 0.01 m, 0.005 m particle are shown in Fig. 3. The particle grid of 0.005 m is in good agreement with the experimental data.

It can be concluded that the simulation results can be trusted when the water particle grid size is almost the same to the object.

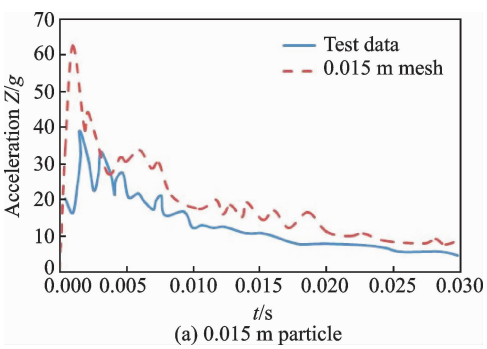

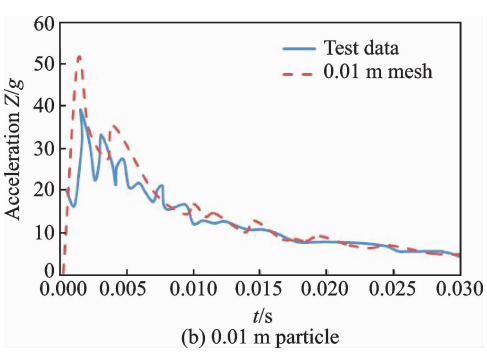

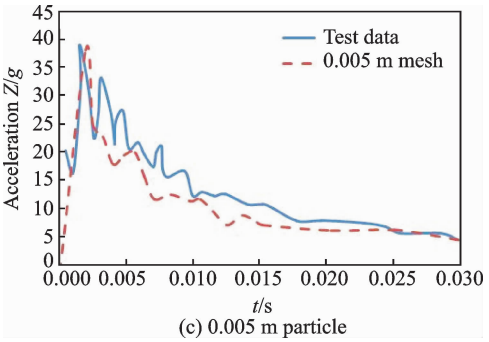

Fig. 3 Vertical acceleration of different particle size

It can figure out that the simulation software and method for helicopter water ditching are feasible.

3 Water Ditching of Helicopter

3.1 Element type and failure criterion

The structure of helicopter can be seen as a thin-wall. There are 4-node quadrilateral and 3-node triangular element types. Because of its high calculation accuracy, Hughes-Liu shell element is applied to deformable structure, which satisfies Kirchhof assumption. Along thickness direction, it is assumed to be uncompressible. The normal of middle surface is still a straight line when deformation.

The beam element involves two basic algorithms: Hughes-Liu and Belytschko-Schwer. Hughes-Liu beam element is a traditional integral element. A set of integral points are adopted to simulate the rectangular or circular cross section. Belytschko-Schwer beam element is an explicit algorithm. It is important that the mesh should be refined in dynamic problem, because the mass distribution is very important in this algorithm.

The deformation of helicopter is mainly the plastic deformation of metal and the failure of composite. The elastic deformation can be considered if the yield limit of the material is not reached. The failure criterion of composite materials is Hashin.

3.2 Parameters and cases of model

The model is simulated by shell and beam element. Specify the mass for concentrated mass

points, then associate them with the structure surrounding. It is shown in Figs. 4,5. Coordinate system is shown in Fig. 6. The plane of $X=0$ is 6.49 mm before the rotor center. The plane of $Y=0$ is symmetry plane of helicopter. The plane of $Z=0$ is the floor of cabin. There are three pressure measuring points arranged in the aircraft belly area, which is shown in Fig. 7.

The materials of helicopter are aluminum alloy, titanium alloy, honeycomb sandwich and carbon fiber composite. Their properties are shown in Tables 3—5. Parameters of Water are shown in Table 6. There are seven cases, including the variety of attitude angle, initial speed, etc.

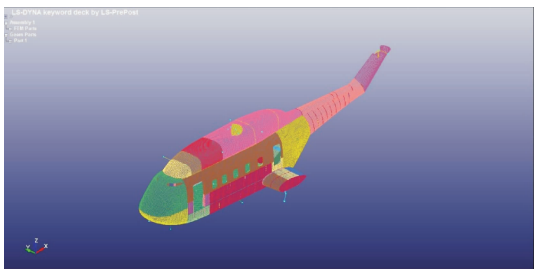

Fig. 4 Shell element with concentrated mass points

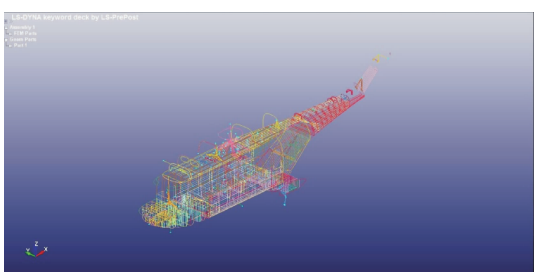

Fig. 5 Beam element with concentrated mass points

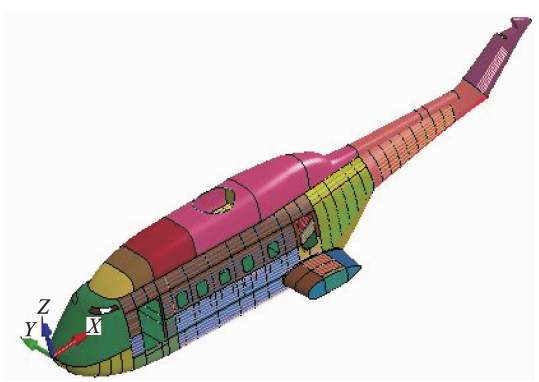

Fig. 6 Coordinate system of helicopter

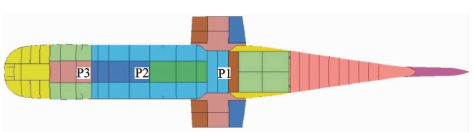

Fig. 7 Location of pressure measuring points

Table 3 Properties of alloy

Parameter	E/GPa	σ_b/MPa	$\sigma_{0.2}$/MPa	τ_b/MPa	μ
2A12/LY12	68	390	270	214	0.3
LD10	71	420	270	214	0.3
7075	71	430	390	258	0.3
TA2	102	490			
0Cr18Ni9	199	569	206		
30CrMnSiA	196	1 080	930	648	0.3
1Cr17Ni2	193	1 080			

Table 4 Properties of carbon fiber composite

Parameter	Value	Parameter	Value
δ/mm	0.285	Y_T/MPa	700
E_{11}/GPa	56	Y_C/MPa	830
E_{22}/GPa	56	S_{12}/MPa	390
μ_{12}	0.094	S_{23}/MPa	350
X_T/MPa	700	S_{13}/MPa	350
X_C/MPa	830		

Table 5 Properties of honeycomb sandwich

Parameter	Value
G_{13}/MPa	47
G_{23}/MPa	36
E_{33}/MPa	484

Table 6 Properties of water

Parameter	Value
Geometry/(m×m×m)	64×12.8×8
Density/(kg·m^{-3})	1 000
Dynamic viscosity/(Pa·s)	0.001 01
Speed of sound in water/(m·s^{-1})	1 484

Table 7 Case of helicopter

Case	V_x/(m·s^{-1})	V_z/(m·s^{-1})	Angle of pitch/(°)	Angle of roll/(°)	Angle of yaw/(°)
1	15.3	3.5	6	0	0
2	15.3	3.5	8	0	0
3	15.3	3.5	10	0	0
4	15.3	3.5	6	−5	0
5	15.3	3.5	8	−5	0
6	15.3	3.5	10	−5	0
7	15.3	3.5	6	0	15

4 Results and Analysis

The acceleration curves, the attitude angle curves and the pressure distribution are achieved of the deformable helicopter. All the curves are filtered using CFC SAE 180[17].

4.1 Case 1

The helicopter touches water at the moment of 0.12 s. The stress at the moment is mainly distributed at the bottom of short wing and the rear of belly. Then, due to nose-down moment, the location of maximum stress moves forward. It moves to the bottom of cockpit at the moment of 0.45 s. The peak overload in the vertical direction is 24.8 m/s^2, which appears at the moment of 0.25 s. The yaw angle changes little. The maximum von-mises effective stress is 218 MPa, so there is no plastic deformation and failure. The maximum pressure distributes in the belly where the stiffness is higher. Three pressure measuring points are arranged in the belly. The pressure curves of P_1, P_2, P_3 are achieved. The peak pressure is 452 376 Pa(Fig. 8).

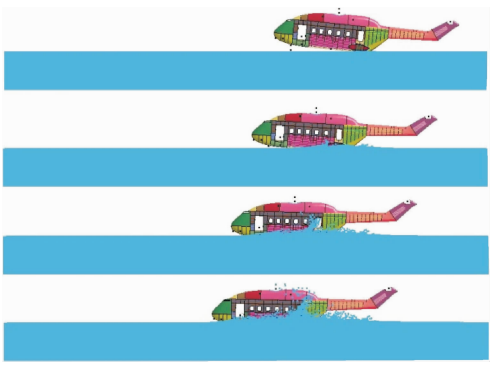

Fig. 8 Attitude of the helicopter and the splash of water at the moment of 0.15, 0.3, 0.45, 0.6 s

4.2 Case 2

The helicopter touches water at the moment of 0.11 s. The stress at the moment is mainly distributed at the bottom of short wing and the rear of belly. Then, due to nose-down moment, the location of maximum stress moves forward. It moves to the bottom of cockpit at the moment of 0.43 s. The peak overload in the vertical direction is 21.7 m/s^2, which appears at the moment of 0.24 s. The maximum pressure distributes in the belly where the stiffness is higher. Three pressure measuring points are arranged in the belly. The peak pressure is 618 992 Pa Figs. 9—16.

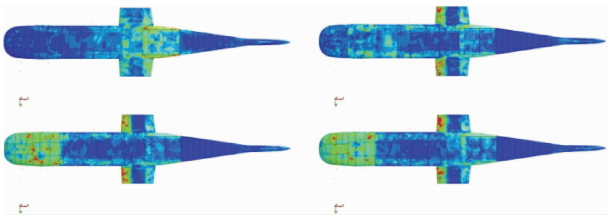

Fig. 9 Contours of stress at the moment of 0.15, 0.3, 0.45, 0.6 s

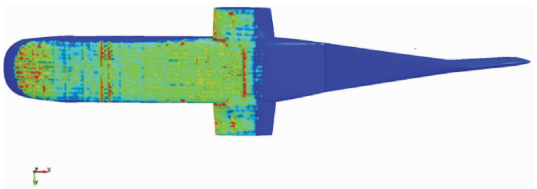

Fig. 10 Contour of peak pressure

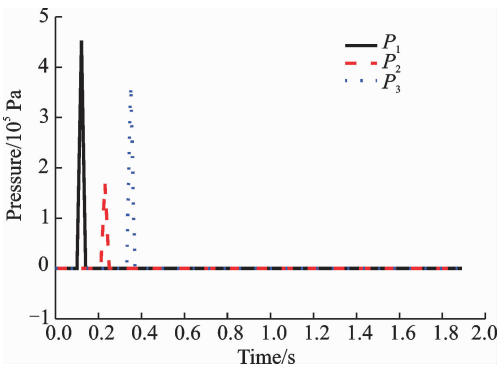

Fig. 11 Curves of pressure at P_1, P_2, P_3

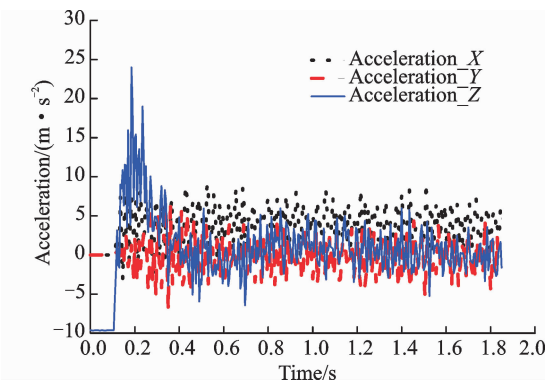

Fig. 12 Curves of acceleration in X, Y, Z direction

4.3 Case 3

The helicopter touches on water at the moment of 0.1 s. The stress at the moment is mainly distributed at the bottom of short wing and the

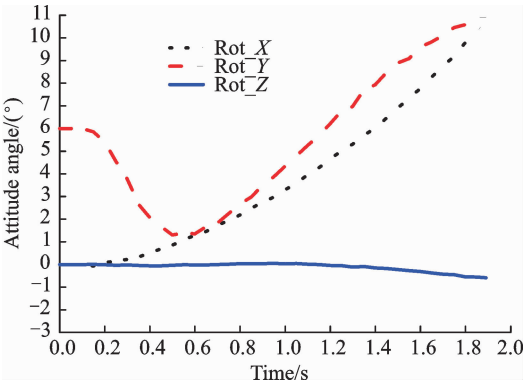

Fig. 13 Curves of attitude angle in X, Y, Z direction

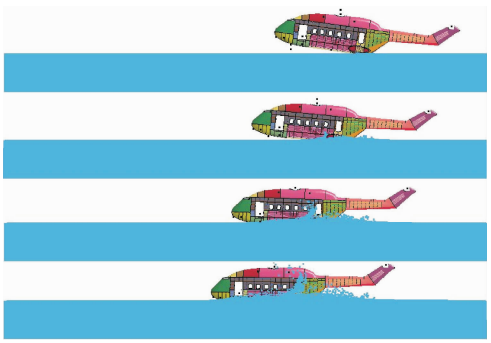

Fig. 14 Attitude of the helicopter and the splash of water at the moment of 0.15, 0.3, 0.45, 0.6 s

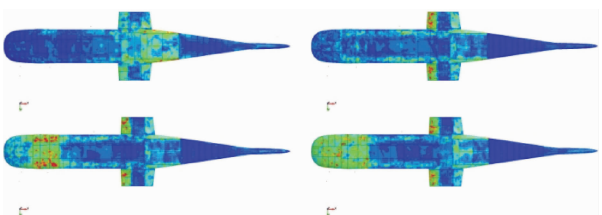

Fig. 15 Contours of stress at the moment of 0.15, 0.3, 0.45, 0.6 s

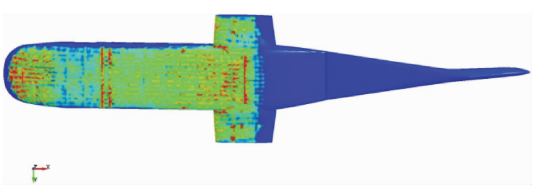

Fig. 16 Contour of peak pressure

rear of belly. Then, due to nose-down moment, the location of maximum stress moves forward. It moves to the bottom of cockpit at the moment of 0.4 s. The peak overload in the vertical direction is 17.2 m/s^2, which appears at the moment of 0.23 s. The peak pressure is 687 746 Pa(Figs. 17—19).

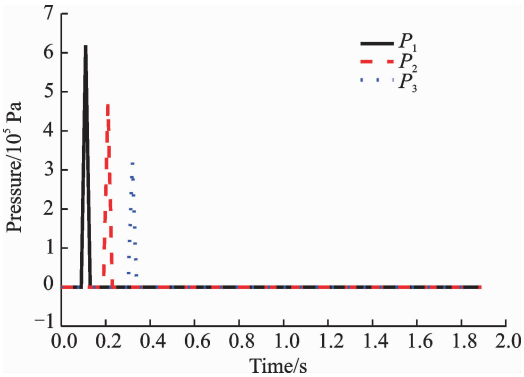

Fig. 17 Curves of pressure at P_1, P_2, P_3

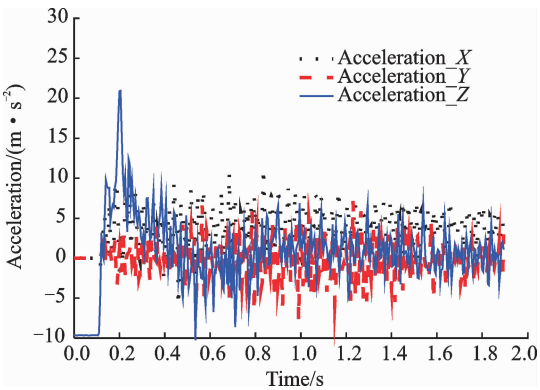

Fig. 18 Curves of acceleration in X, Y, Z direction

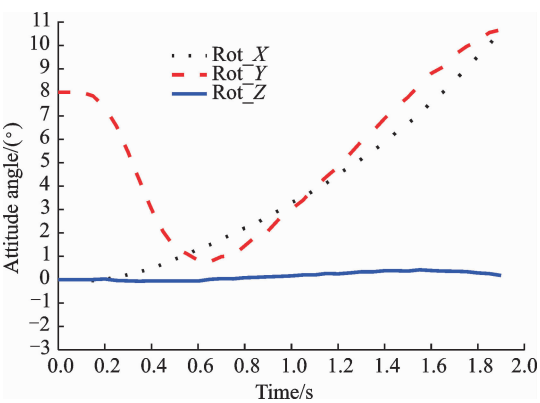

Fig. 19 Curves of attitude angle in X, Y, Z direction

4.4 Case 4

The helicopter touches water at the moment of 0.08 s. The stress at the moment is mainly distributed at the bottom of left short wing. Then, due to nose-down moment and rolling moment, the location of maximum stress moves forward and right. The peak overload in the vertical direction is 13.2 m/s^2, which appears at the moment of 0.2 s. The yaw angle changes larger. It becomes unstable. The peak pressure is 442 478 Pa(Figs. 20—26).

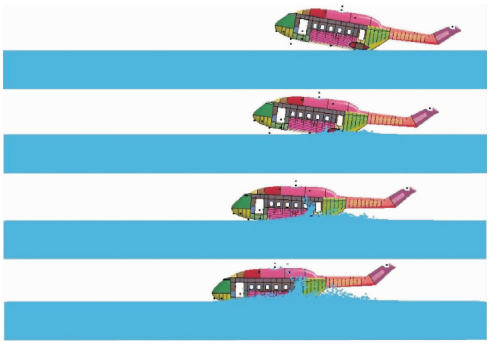

Fig. 20 Attitude of the helicopter and the splash of water at the moment of 0.15, 0.3, 0.45, 0.6 s

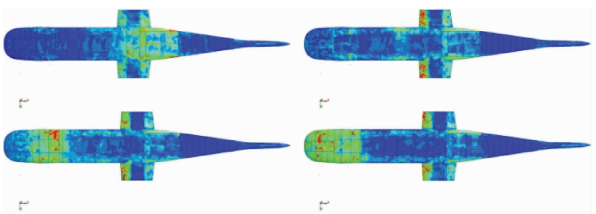

Fig. 21 Contours of stress at the moment of 0.15, 0.3, 0.45, 0.6 s

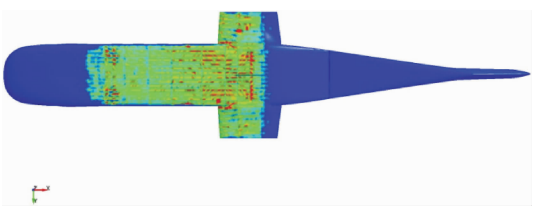

Fig. 22 Contour of peak pressure

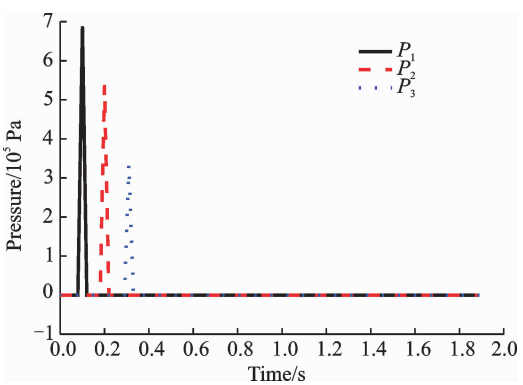

Fig. 23 Curves of Pressure at P_1, P_2, P_3

4.5 Case 7

The helicopter touches water at the moment of 0.12 s. The stress at the moment is mainly distributed at the bottom of left short wing and the rear of belly. Then, due to nose-down moment and yawing moment, the location of maximum stress moves forward. The peak overload in the vertical direction is 15.1 m/s^2, which appears at the moment of 0.25 s. The yaw angle and roll angle changes larger. It becomes very unstable. The peak pressure is 432 323 Pa(Figs. 27—29).

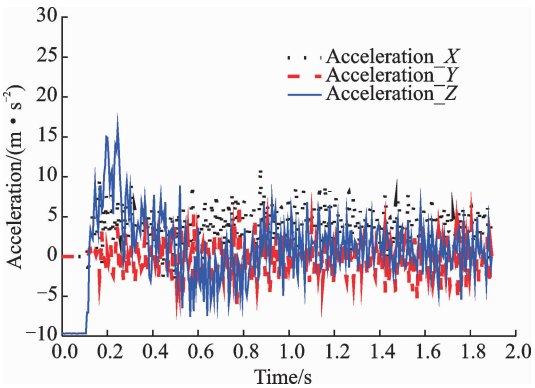

Fig. 24 Curves of acceleration in X, Y, Z direction

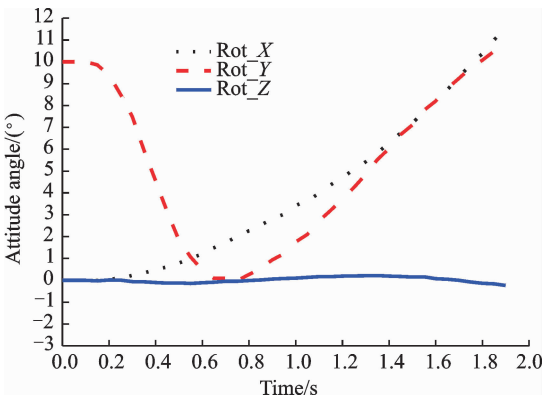

Fig. 25 Curves of attitude angle in X, Y, Z direction

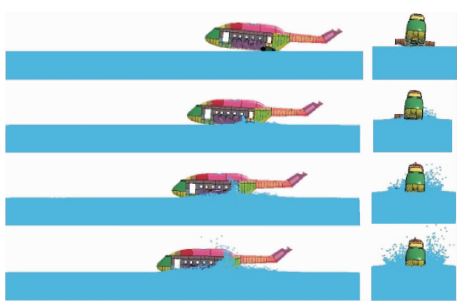

Fig. 26 Attitude of the helicopter and the splash of water at the moment of 0.15, 0.3, 0.45, 0.6s

4.6 Different pitch angle

The curves of vertical acceleration of helicopter with pitch angles of 6°, 8°, and 10° are shown in Fig. 38.

It can figure out that vertical peak accelera-

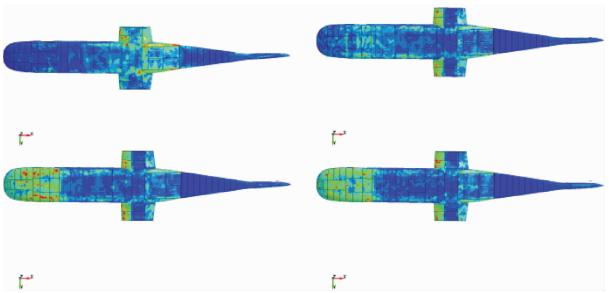

Fig. 27 Contours of stress at the moment of 0.15, 0.3, 0.45, 0.6 s

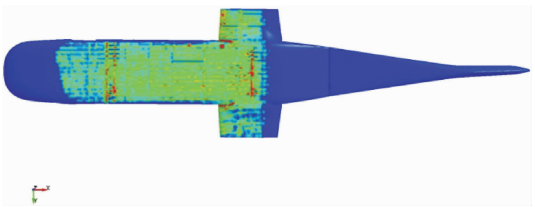

Fig. 28 Contour of peak pressure

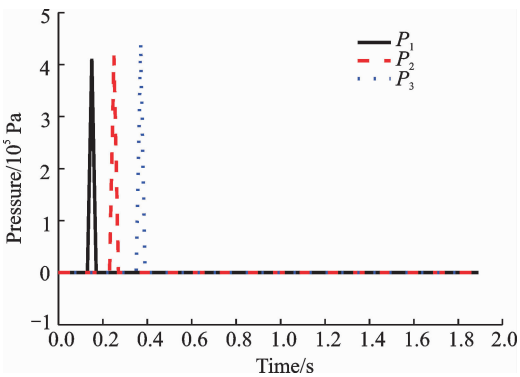

Fig. 29 Curves of Pressure at P_1, P_2, P_3

tion is decreased with the increase of the pitch angle. Therefore, increase the pitch angle appropriately can reduce the peak overload of helicopter (Figs. 30—38).

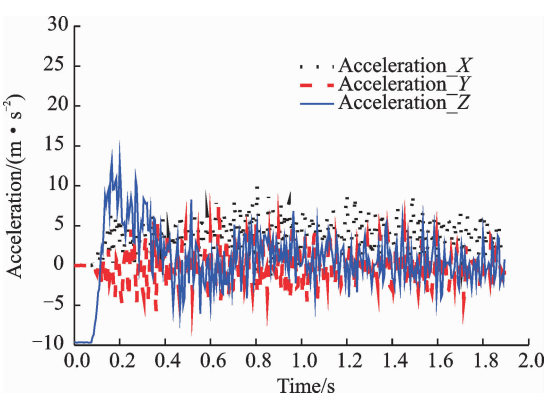

Fig. 30 Curves of acceleration in X,Y,Z direction

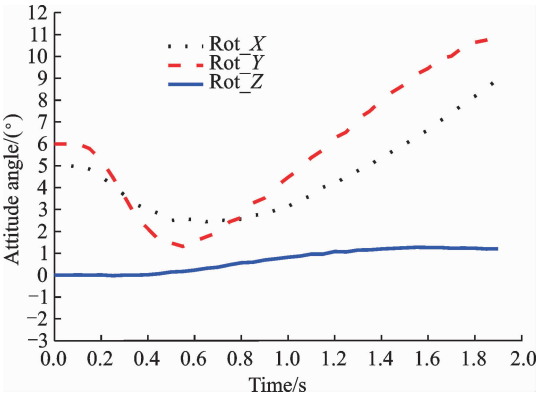

Fig. 31 Curves of attitude angle in X,Y,Z direction

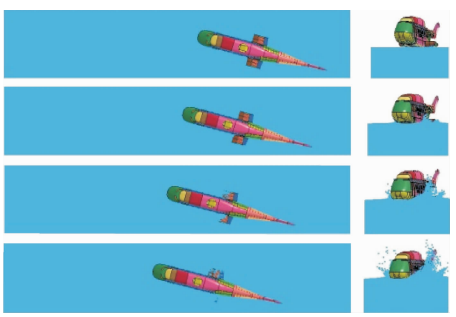

Fig. 32 Attitude of the helicopter and the splash of water at the moment of 0.15, 0.3, 0.45, 0.6 s

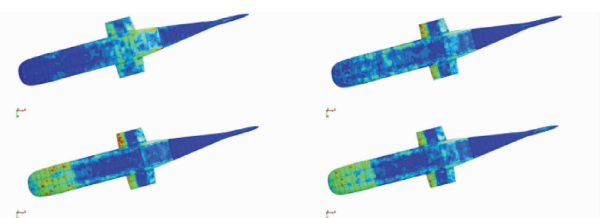

Fig. 33 Contours of stress at the moment of 0.15, 0.3, 0.45, 0.6 s

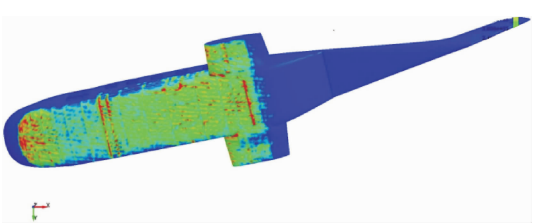

Fig. 34 Contour of peak pressure

4.7 Different roll angle

The curves of vertical acceleration of helicopter with roll angles of 0° and 5° are shown in Fig. 39. Curves of attitude angle in X,Y,Z direction with roll angles 0° and 5° are shown in Fig. 40.

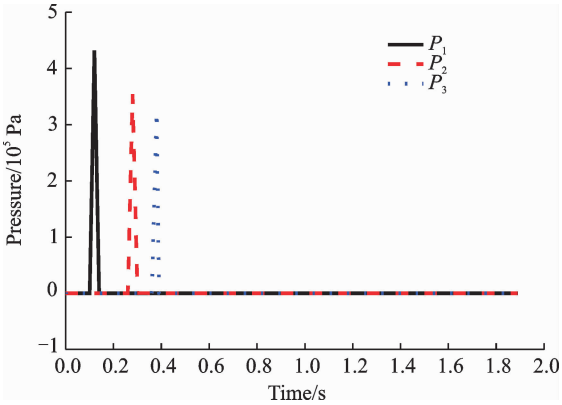

Fig. 35 Curves of pressure at P_1, P_2, P_3

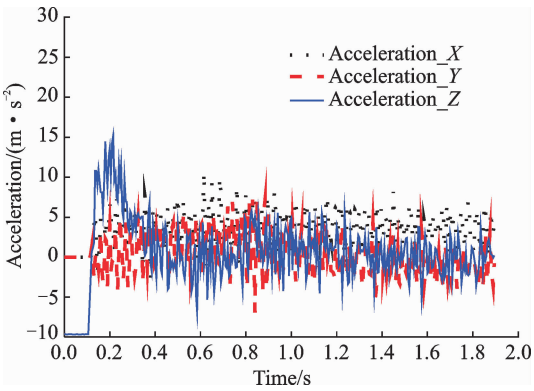

Fig. 36 Curves of acceleration in X, Y, Z direction

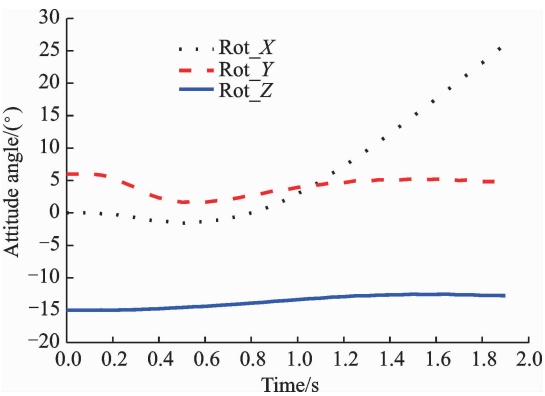

Fig. 37 Curves of attitude angle in X, Y, Z direction

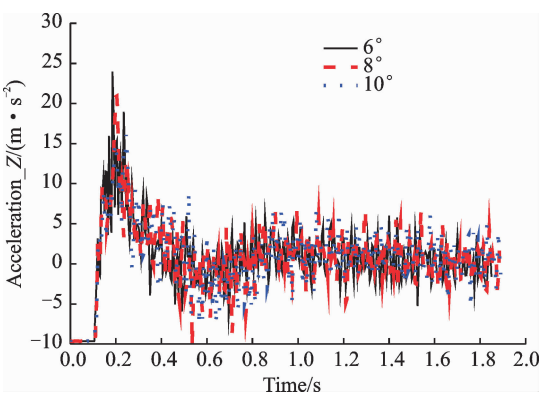

Fig. 38 Curves of vertical acceleration of helicopter with pitch angle 6°, 8°, and 10°

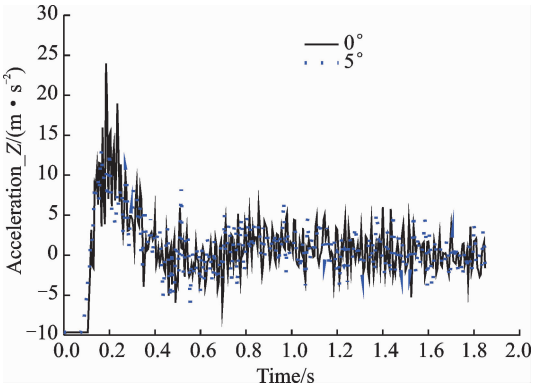

Fig. 39 Curves of vertical acceleration of helicopter with roll angle 0° and 5°

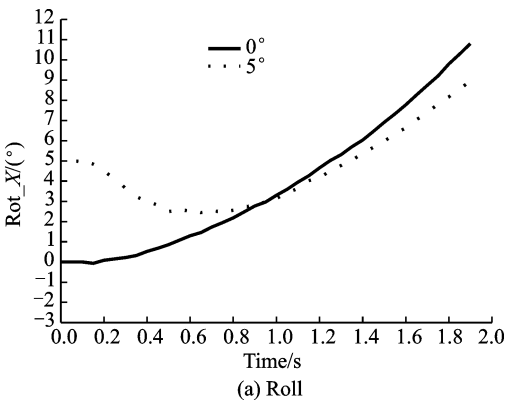

(a) Roll

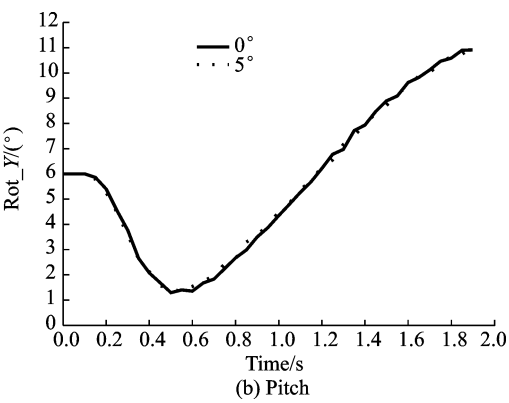

(b) Pitch

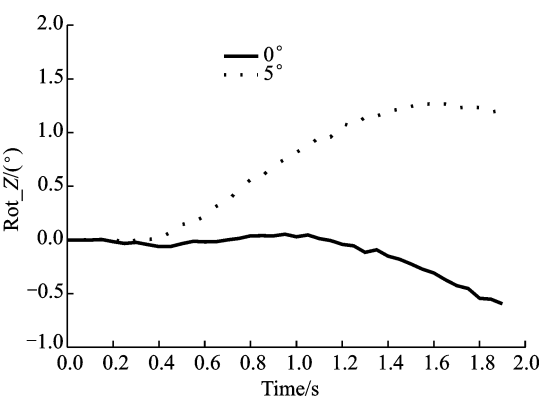

(c) Yaw

Fig. 40 Curves of attitude angle in X, Y, Z direction with roll angle 0° and 5°

It can figure out that vertical peak acceleration is decreased with the roll angle, because the area of helicopter contact with water decreaseds at the beginning. But ditching becomes unstable for the yaw angle increases a lot.

4.8 Different yaw angles

The curves of vertical acceleration of helicopter with yaw angles of 0° and 15° are shown in Fig. 41. Curves of attitude angle in X,Y,Z direction with yaw angles 0° and 15° are shown in Fig. 42.

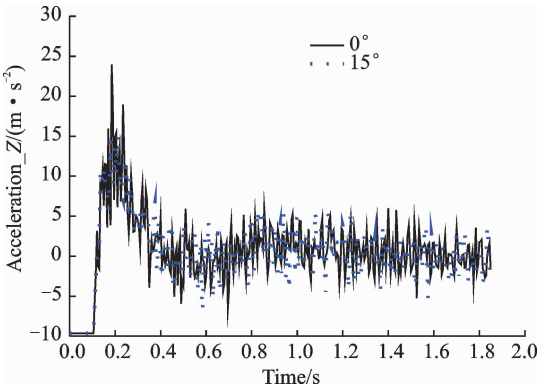

Fig. 41 Curves of vertical acceleration of helicopter with yaw angle 0° 15°

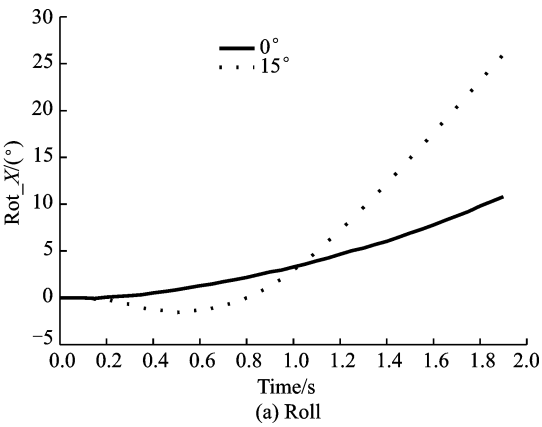

(a) Roll

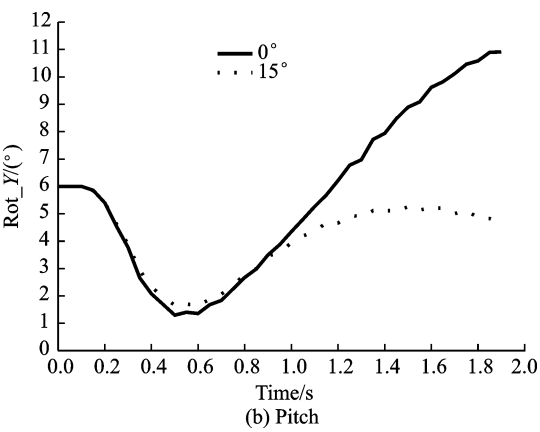

(b) Pitch

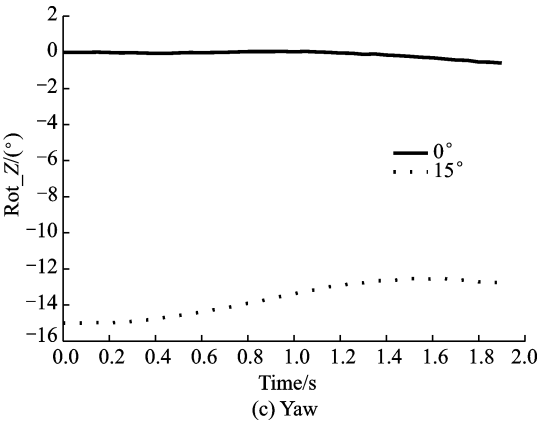

(c) Yaw

Fig. 42 Curves of attitude angle in X,Y,Z direction with yaw angle 0° and 15°

It can figure out that vertical peak acceleration is decreased with the yaw angle. But the ditching becomes very unstable for the yaw angle and roll angle increases a lot.

5 Comparative Analysis of Simulation and Experimental Results

The experiment of helicopter water ditching is carried out by a Russian institution. It returns the data of Cases 1—7. The peak vertical acceleration is compared, which is shown in Table 8.

Table 8 Comparison of simulation and experimental data

Case	Peak acceleration of simulation/ ($m \cdot s^{-2}$)	Peak acceleration of experiment/ ($m \cdot s^{-2}$)	Difference/ %
1	24.8	28.7	−13.59
2	21.7	24.4	−11.07
3	17.2	18.6	−7.53
4	13.2	15.2	−13.16
5	11.2	12.1	−7.44
6	9.3	10.2	−8.82
7	15.1	13.9	8.63

The trend of simulation and experimental results is similar, which proves that the simulation results are credible.

6 Conclusions

(1) The validity of water ditching method for kinds of this problem is verified. The rationality and correctness of this method is proved.

(2) Different attitude of helicopter water ditching are simulated. The curves of acceleration and

curves of attitude angles in X, Y, Z direction are achieved. Three pressure measuring points are arranged in the aircraft belly area. The effects of attitude on helicopter water ditching are discussed, particularly the stability and overload of helicopter. Through the contours of stress, the maximum pressure distributes at the position of aircraft belly where stiffness is larger. Roll angle and yaw angle have disadvantage on water ditching.

(3) Simulation and experimental results are compared. The difference of the peak load is small, which proves that the simulation method is feasible.

Acknowledgments

This work was funded by the International S&T Cooperation Program of China (No. 2011DFR80210) and the National Natural Science Foundation of China (No. 11302105).

References:

[1] NRS TOSO. Contribution to the modelling and simulation of aircraft structures impacting on water[D]. France: Universität Stuttgart, 2009.

[2] BROOKS J R, ANDERSON L A. Dynamics of a space module impacting water[J]. Journal of Spacecraft and Rockets, 1994, 31(3): 509-515.

[3] STRECKWALL H, LINDENAU O, BENSCH L. Aircraft ditching: A free surface/ free motion problem[J]. Archives of Civil and Mechanical Engineering, 2007,7(3): 177-190.

[4] TOSO-PENTECOTE N, DELSART D, VAGNOT A. Assessment of the SPH method: Simulation of simple body shapes impacting on water and a PUMA helicopter ditching[C]// ODAS 10th ONERA-DLR Symposium. Berlin: Deutsches Zentrum für Luft und Raumfahrt, 2009.

[5] GROENENBOOM P H L, CARTWRIGHT B K. Hydrodynamics and fluid-structure interation by coupled SPH-FE method[J]. Journal of Hydraulic Research, 2010 48(1): 61-73..

[6] GUO B D, QU Q L, LIU P Q. Ditching performance of silent aircraft SAX-40 in hybrid wing-body configuration[J]. Chinese Journal of Aeronautics, 2013, 34(11): 2443-2451. (in Chinese)

[7] FANG C. Simulation of fluid-solid interaction on water ditching of an airplane by ALE method[D]. Shanghai: Fudan University, 2011. (in Chinese)

[8] YAN J Y. Research on aeroplane ditching numerical simulation based on SPH method[D]. Nanjing: Nanjing University of Aeronautics and Astronautics, 2012. (in Chinese)

[9] ZHU X Y. Numerical analysis on strength of airliner ditching[D]. Wuhan: Wuhan University of Technology, 2012. (in Chinese)

[10] SHEN R H, DU X W, WAN Z M. Structure design and buffer simulation of airbag buffer system for lunar probe[C]// 2nd Academic Conference of Professional Committee of Space Exploration Technology. Beijing: Chinese Space Institute, 2005: 321-327. (in Chinese)

[11] LI M Q. Numerical analysis and experimental research on ditching characteristic of emergency floatation bags[D]. Nanjing: Nanjing University of Aeronautics and Astronautics, 2008. (in Chinese)

[12] SUN W M. The research on civil aircraft fuselage structural stability and the ditching[D]. Nanjing: Nanjing University of Aeronautics and Astronautics, 2009. (in Chinese)

[13] HE T, YANG J. 10.0/LS-DYNA ANSYS nonlinear finite element analysis examples guidance[M]. Beijing: China Machine Press, 2007. (in Chinese)

[14] HAN X. Smoothed particle hydrodynamics: A mesh free particle method[M]. Changsha: Hunan University Press, 2005. (in Chinese)

[15] LIU Z B. The simulation analysis and experimental verification of the airbag cushioning system for Mars landing process[D]. Changsha: Hunan University, 2014. (in Chinese)

[16] JACKSON K E, FUCHS Y T. Comparison of ALE and SPH simulations of vertical drop tests of a composite fuselage section into water[C]//10th International LS-DYNA Users Conference. Dearborn: Livemore Software Technology Corporation, 2008: 1-20.

[17] Society of Automotive Engineers (SAE). Recommended Practice: Instrumentation for Impact Test - Part 1[S]. Electronic Instrumentation, SAE J211/1, March 1995.

Dr. **Sun Xuan** received the B. S. degree in aircraft designing from Beihang University, Beijing, China, in 2004 and 2008, and Ph. D. degree in aircraft designing from Nanjing University of Aeronautics and Astronautics, Nanjing, China, in 2009 and 2016. In July 2016, he joined the System Design Institute of Hubei Aerospace Technology Academy, China Aerospace Science and Industry Corporation, as a researcher. His research is focused on system design of air-

craft and CFD algorithm.

Prof. **Tong Mingbo** received the B. S. degree in aircraft designing from Northwestern Polytechnical University, Xi′an, China, and the Master degree in aircraft designing from Nanjing University of Aeronautics and Astronautics, Nanjing, China, and the Ph. D. degree in aircraft designing from Beihang University, Beijing, China. From 1996 to present, he has been with the College of Aerospace, Nanjing University of Aeronautics and Astronautics (NUAA), where he is currently a full professor and executive director of the Ministerial Key Discipline Laboratory of Advanced Design Technology of Aircraft. His research has focused on system designing and CFD algorithm.

Mr. **Wang Zhengzhong** received the B. S. degree in aircraft designing from Hunan University, Hunan, China, in 2000 and 2004, and Master degree in missle designing from Harbin Institute of Technology, Harbin, China, in 2004 and 2006. In July 2006, he joined the System Design Institute of Hubei Aerospace Technology Academy, China Aerospace Science and Industry Corporation, as a researcher. His research is focused on system design of aircraft and CFD simulation.

(Executive Editor: Zhang Bei)